Surface & Coatings Technology 202 (2008) 5162–5169

Contents lists available at ScienceDirect

Surface & Coatings Technology

journal homepage: www.elsevier.com/locate/surfcoat

Carbon nanotube reinforced aluminum composite coating via cold spraying

Srinivasa R. Bakshi [a], Virendra Singh [c], Kantesh Balani [a], D. Graham McCartney [b], Sudipta Seal [c], Arvind Agarwal [a,*]

[a] Department of Mechanical and Materials Engineering, Florida International University, Miami, FL 33174, USA
[b] School of Mechanical, Materials and Manufacturing Engineering and Management, University of Nottingham, University Park, Nottingham, NG7 2RD, UK
[c] AMPAC, Nanoscience and Technology Center (NSTC) and Mechanical, Materials and Aerospace Engineering, University of Central Florida, Orlando, FL 32816, USA

ARTICLE INFO

Article history:
Received 20 February 2008
Accepted in revised form 22 May 2008
Available online 3 June 2008

Keywords:
Cold spraying
Carbon nanotubes
Aluminum
Composites
Elastic modulus

ABSTRACT

Multiwalled carbon nanotube (CNT) reinforced aluminum nanocomposite coatings were prepared using cold gas kinetic spraying. Spray drying was used to obtain a good dispersion of the nanotubes in micron-sized gas atomized Al–Si eutectic powders. Spray dried powders containing 5 wt.% CNT were blended with pure aluminum powder to give overall nominal CNT compositions of 0.5 wt.% and 1 wt.% respectively. Cold spraying resulted in coatings of the order of 500 μm in thickness. Fracture surfaces of deposits show that the nanotubes were uniformly distributed in the matrix. Nanotubes were shorter in length as they fractured due to impact and shearing between Al–Si particles and the Al matrix during the deposition process. Nanoindentation shows a distribution in the elastic modulus values from 40–229 GPa which is attributed to microstructural heterogeneity of the coatings that comprise the following: pure Al, Al–Si eutectic, porosity and CNTs.

1. Introduction

Cold spraying is a relatively new coating technique wherein powder particles are accelerated to supersonic velocities (600–1500 m/s) by a carrier gas flowing under large pressure difference (up to 3.5 MPa) through a de Laval type of nozzle and made to impact onto a substrate [1]. It has unique advantages like minimal effects on the material sprayed like oxidation, grain coarsening or phase changes, produces highly dense coatings and that the substrate is not affected during the coating process. The disadvantage is that a large amount of carrier gas is lost, unless recycled, and that only plastically deformable materials can be deposited. There is no melting of the particles and the bonding is believed to be due to adiabatic shear instabilities arising from thermal softening at the particle/substrate and particle/particle interfaces which have been modeled using finite element method [2,3]. The constitutive relations for plastic flow used in modeling the deformation and bonding take care of the dependence of the flow stress on the strain, strain rate, temperature and pressure. The parameters affecting the process and spraying efficiency are particle size, density of particles, temperature of gas, density of gas and spraying angle, and various models have been proposed for the effect of various parameters [4–6]. Cold spraying has been used to deposit many types of materials including pure metals [7–11], alloys [12–15] and composite materials [16–19]. In all the above cases of spraying composite coatings, it was observed that the second phase was distributed uniformly within the matrix. Recently there has been interest in cold spraying composites containing nanofillers as reinforcements by cold spraying [18,19].

Since the discovery of carbon nanotubes (CNTs) by Iijima in 1991, a lot of interest has been devoted to the application of CNTs as reinforcement for polymer [20–22], ceramic and metal matrix composites. This is due to excellent mechanical properties of CNT like strength and stiffness up to 63 GPa and ~1 TPa respectively [23] and thermal conductivity of up to 3000 W/m K [24]. The use of CNTs as reinforcements increases the strength and stiffness of metals and polymers, while it leads to an improvement in the fracture toughness [25,26] and thermal conductivity [27] of ceramics. Some of the processing techniques used in fabrication of CNT reinforced MMC are conventional powder metallurgy techniques [28,29], electroplating [30] and electroless plating [31] from CNT-containing electrolytic baths, spark plasma sintering [32,33], mechanical alloying [34] and thermal spraying [35,36]. Uniform dispersion and alignment of nanotubes within the metal matrix composites is still a challenge. Recently some success has been obtained in the alignment and dispersion of nanotubes and nanowires in blown bubble films of epoxies containing dispersed CNTs [37].

The overall aim of the work was to utilize the technique of cold gas spraying to investigate microstructure development from a blended feedstock of pure aluminum powder and an agglomerated powder comprising aluminum–silicon eutectic alloy and CNTs prepared by

* Corresponding author.
E-mail address: agarwala@fiu.edu (A. Agarwal).

0257-8972/$ – see front matter © 2008 Elsevier B.V. All rights reserved.
doi:10.1016/j.surfcoat.2008.05.042

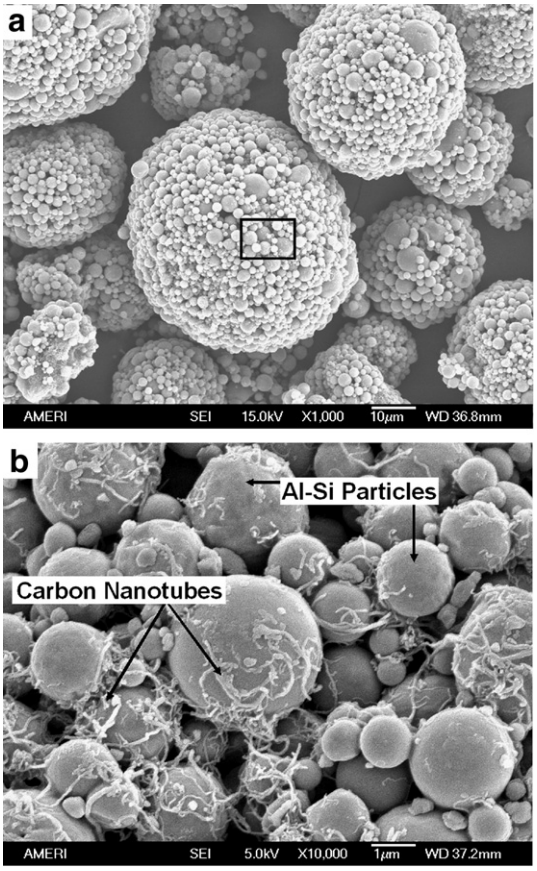

Fig. 1. SEM micrograph showing a) spray dried Al–Si agglomerate and b) magnified region within the rectangle in a) showing CNTs within the agglomerate.

spray drying. A major challenge in the manufacture of CNT-containing metal matrix composites is distributing the CNTs uniformly and it was for this reason that the agglomerates of CNTs and eutectic Al–Si powder were employed. Individual agglomerates of this mixture have the potential to fragment on impact during spraying, releasing the CNTs. The use of pure aluminum instead of the Al–Si powder in the agglomerated feedstock might cause concentrated CNT regions to form because of the greater plasticity of pure aluminum and so was not explored in the present study.

2. Experimental details

2.1. Cold spraying rig

Cold spraying experiments were carried out at the University of Nottingham which has an in-house built system comprising a high pressure gas supply, high pressure powder feeder, a converging–diverging nozzle and an *X*–*Y* traverse unit. The design of the cold spray rig is described in detail elsewhere [38]. The powder feeder used was a Praxair 1264HP (Praxair Surface Technologies, Indianapolis, IN) which has a maximum pressure capability of 3.4 MPa. Helium gas was used as the main gas and for the current work, a main gas stagnation pressure of 2.9 MPa was employed. Nitrogen gas was used as the powder carrier gas and the pressure was kept 0.1 MPa higher than that of the main gas in order to facilitate the injection of the powder into the jet. The nozzle was fixed to a frame and the substrate was fixed onto an *X*–*Y* traverse table, the movement of which was programmable using a computer. Eight layers were sprayed to build up the coating thickness. The substrate used was 6061 aluminum alloy which was grit blasted prior to spray deposition.

2.2. Powder feedstock

Aluminum–silicon (Al–Si) eutectic alloy powder of composition Al–11.6% Si–0.14% Fe by weight and mean particle size 2.4±1.2 μm was obtained from Valimet Inc. (Stockton, CA, USA). Multiwalled carbon nanotubes (CNT), obtained from Inframat Advanced Materials (Willington, CT, USA), had a purity of more than 95% and diameter of 40–70 nm and length 1–3 μm. Spray drying was used to disperse the carbon nanotubes (CNTs) within the agglomerates of fine sized Al–Si eutectic alloy powders. The spray dried agglomerates had a particle size of 57±21 μm. The spray dried powders contained 5 wt.% CNT and will be referred to as SD Al–5CNT powder hereafter. The SD Al–5CNT powder was mixed with 99.7% pure Al powder (particle size of 26±13 μm Alpoco, Minworth, UK) in proportions of 10 wt.% and 20 wt.% to generate powders for spraying which contained an overall CNT content of 0.5 wt.% and 1 wt.% respectively. The mixing of pure aluminum powder and SD Al–5CNT was carried out in a turbula mixer for 1 h.

2.3. Microstructural and mechanical characterization

The external morphology of powder samples was examined in a scanning electron microscope (SEM). Samples were prepared by sprinkling the loose powder on an adhesive tab and then examined using secondary electron imaging mode using either a Jeol JSM 630OF or FEI XL 30 FEG-SEM. To examine coating cross-sections samples were cut using a high speed cutting saw and were mounted in hot mounting resin. They were then ground and polished to a 0.1 μm finish using colloidal silica. For examination in an optical microscope they were etched in Keller's reagent (5 ml HNO_3, 3 ml HCl, 2 ml HF and 190 ml H_2O). Porosity was determined from the optical micrographs of the polished cross-sections of the coatings by calculating the fractional area occupied by the pores. A total of seven micrographs at magnifications ranging from 100x to 400x were analyzed using image analysis software Image J. Coating fracture surfaces were prepared by breaking a part of the coating under tension and attaching to an SEM stub in such a manner that the fracture surface was at an angle to the normal. The length and diameter of CNTs were measured from representative SEM micrographs using Image J. Length and diameter were reported as the average of 20–50 measurements. A Philips/FEI Tecnai F30 field emission gun transmission electron microscope (TEM) operating at an accelerating voltage of 300 kV was used to study the microstructure of the deformed matrix as well as the condition of the nanotubes at high resolution. The samples for TEM were in the form of a 3 mm disc, which were punched from the coating less than 100 μm thick prepared by grinding on a 600 grit abrasive paper, followed by dimpling at the center using a dimple

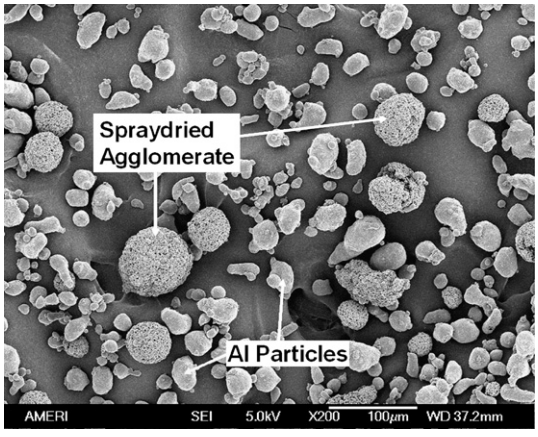

Fig. 2. SEM micrograph of mixture of pure Al and 10 wt.% SD Al–5CNT powder.

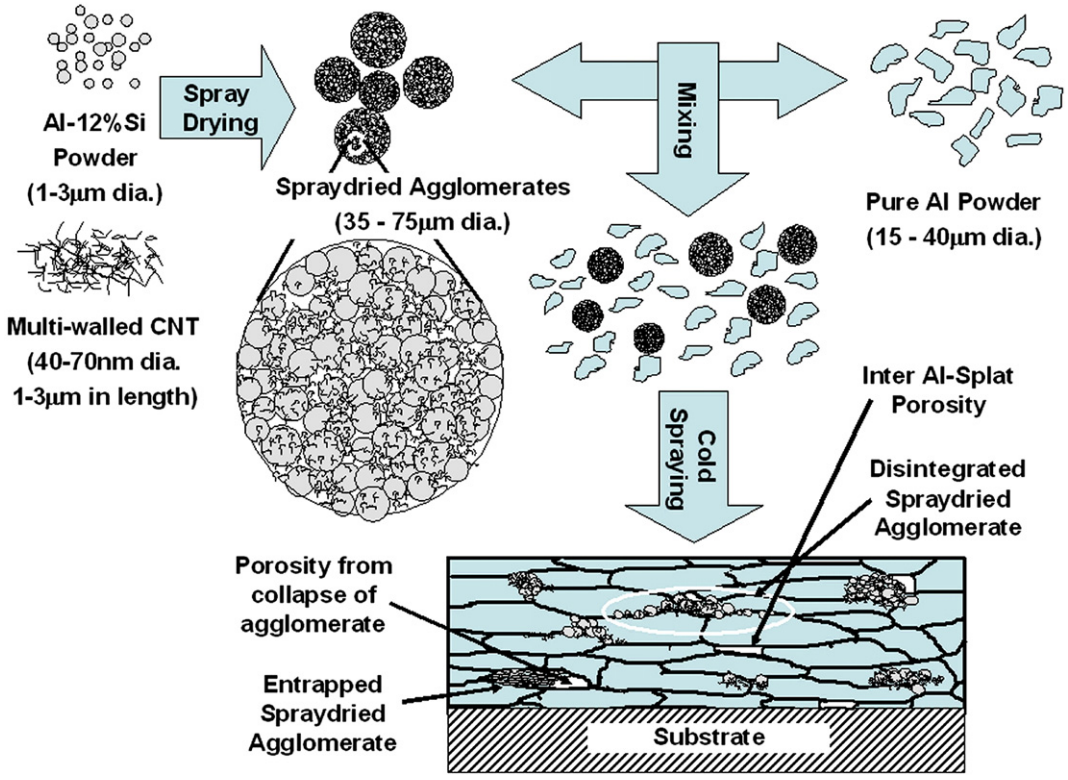

Fig. 3. Schematic of the steps involved in the fabrication of the composite coating.

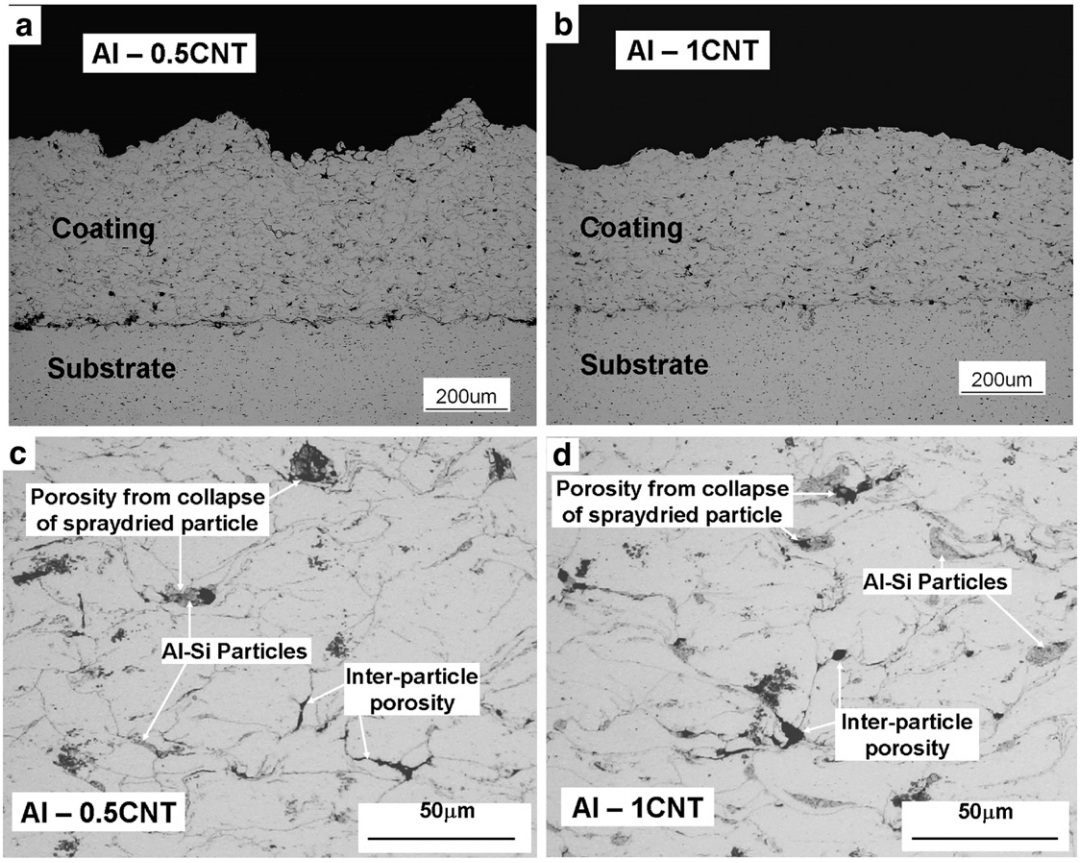

Fig. 4. Optical micrograph of a) Al–0.5CNT coating and b) Al–1CNT coating and high magnification images of c) Al–0.5CNT and d) Al–1CNT.

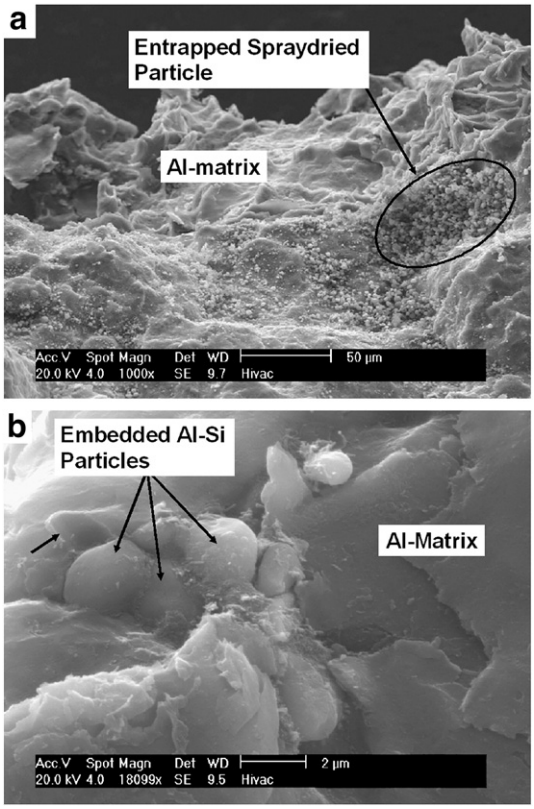

Fig. 5. SEM micrograph of Al–0.5 CNT coating showing a) entrapped spray dried particle in Al matrix, and b) high magnification image showing embedding of Al–Si particles in Al matrix.

grinder (Model 656 Mk3, Gatan, Inc., CA, USA). The final thinning was carried out by twinjet polishing (Model 110, E.A. Fischione Instruments, Inc., PA, USA) using a 30 vol.% mixture of 6 N HNO_3 in ethanol as the electrolyte until a hole was formed. Nanoindentation was carried out using Hysitron Triboindendenter (Hysitron, Inc., Minneapolis, MN, USA) to measure the elastic modulus of the composite coatings. A Berkovich indenter of tip radius 40 nm was employed. The load function comprised a linear increase in load up to 600 µN in 10 s followed by a 2 s halt at maximum load and followed by a linear decrease in load to zero in 10 s.

3. Results and discussion

3.1. Powder characterization

Fig. 1 shows the SEM micrograph of the spray dried particles. It can be seen that the CNTs were dispersed uniformly in the agglomerate. The extent of clustering of CNT was reduced by spray drying. CNTs are coated with the binder used in spray drying which is typically an aqueous solution of polyvinyl alcohol. Wetting of the CNTs by the binder might be one reason for the good dispersion observed. The spray dried powder forms as a result of the evaporation of water from the atomized droplet. Therefore, the nanotubes which are dispersed in the slurry appear relatively uniformly distributed over the Al–Si particle surface. The spray dried agglomerates contain a significant amount of porosity since they are formed by packing of rigid spheres. Fig. 2 shows a SEM image of the blended mixture containing 10 wt.% of the SD Al–5CNT powder. It can be seen that both the pure Al and the spray dried powders have mixed intimately. Pure aluminum powders are slightly elongated in shape in comparison to spherical SD Al–5CNT agglomerates.

3.2. Cold spraying

Cold spraying of the powder mixtures were carried out onto AA6061 substrate. The mixture of Al and SD Al–5CNT sprayed well. This is attributed to the high deposition efficiency of non-porous and readily deformable Al powder. It is possible to entrap the Al–Si particles and the nanotubes resulting from the disintegration of the spray dried agglomerates in between the deforming Al particles. Composite coatings containing an overall nominal CNT content of 0.5 wt.% and 1 wt.% and having a thickness of ~500 µm were prepared. These coatings will be referred as Al–0.5CNT and Al–1CNT hereafter. Fig. 3 shows a schematic illustration of the powder pretreatment steps involved in the fabrication of the composite coating. The velocity attained by the particles during cold spraying is given by Dykhuizen [39] as

$$V_p = V\sqrt{\frac{C_D A_p \rho x}{m}} \quad (1)$$

where V is the gas velocity, C_D is the drag coefficient, A_p is the cross-section area of the particle, m is the mass of the particle and x is axial position. The energy of the impact is absorbed in disintegration of the agglomerates with only a fraction of the kinetic energy available for plastic deformation of individual Al–Si particles. There are only a few studies on the impact breakage of agglomerates [40,41]. In these studies, breakage of agglomerates has been simulated using Distinct Element Method (DEM). Thornton et al.[40] have simulated the breakage of an agglomerate of 1000 particles having a radius, solid density, Young's modulus and Poisson's ratio of 100 µm, 2650 kg m^{-3}, 70 GPa and 0.3 respectively which are close to the properties of the Al–Si eutectic alloy. The coefficient of friction and surface energy were assumed as 0.35 and 3.0 J m^{-2} respectively. It was concluded that for velocities of impact of 1 m s^{-1} there is extensive damage to the

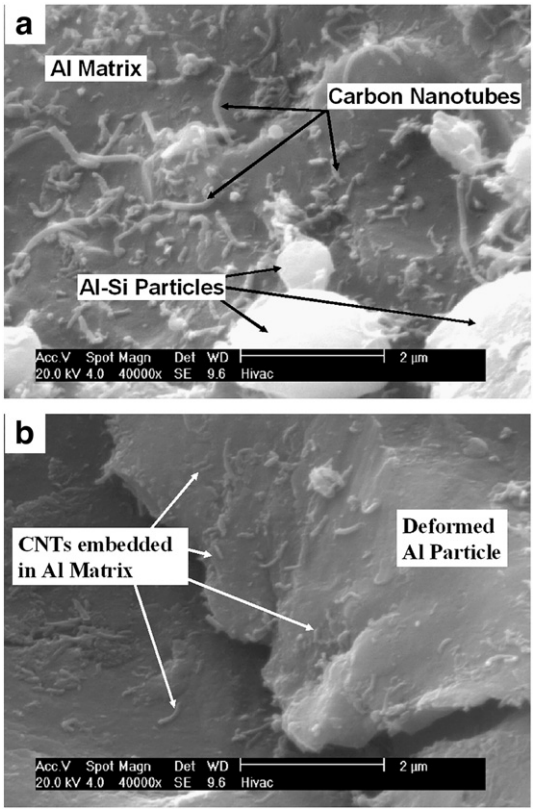

Fig. 6. SEM of fracture surface showing a) good distribution of nanotubes, and b) CNTs embedded in Al particle.

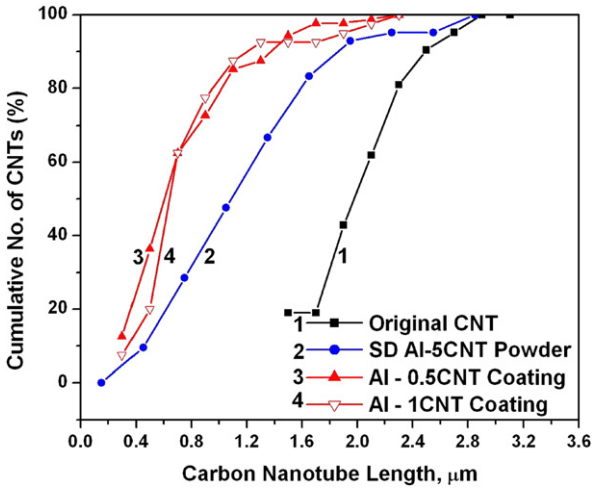

Fig. 7. Length of the CNTs at various stages in the fabrication process.

structure [40]. Hence, it is expected that under the high velocity (~600 m s^{-1}) impact in cold spraying the spray dried particles will disintegrate.

3.3. Microstructure of the coatings

Fig. 4 shows optical micrographs of the Al–0.5CNT and Al–1CNT coatings. It can be seen that thick and dense coatings of the order of 500 μm were formed by cold spraying. Three distinct features seen in the optical micrographs are: deformed Al particles; Al–Si particles from collapse of the spray dried particles; and porosity. As seen in Fig. 4c and d, the Al–Si particles were found in between the deformed Al particles. Al particles had undergone a large amount of plastic flow to form elongated disc like particles which are often referred to as splats. Papyrin et al. [42] have measured the plastic strain (ε_p) in the individual particles from the deformed shape of cold spray deposited single particles and have correlated it empirically to the material properties and the velocity of the particles as follows.

$$\varepsilon_p = exp\left(-1.4\frac{H_p}{\rho_p \nu_p^2}\right) \quad (2)$$

Here ε_p is the strain in the particle, H_p is the hardness of the particle (MPa) and ρ_p and ν_p are the density and velocity of the particles on impact respectively. The velocity of the Al particles measured by laser particle image velocimetry under similar conditions was found to be 636±20 m s^{-1} [43]. The measured hardness of the aluminum powder particles was found to be 315 MPa and so from Eq. (2) the corresponding plastic strain in the particles comes out to be 0.66 which is a very significant degree of plastic deformation. Under similar conditions, the strain of an Al–Si particle having a hardness of 1260 MPa comes out to be 0.19. So it is expected that the Al–Si particles will undergo much lower amounts of deformation due to impact (assuming that the particles adhered and did not disintegrate or rebound).

The porosity for the Al–0.5CNT and Al–1CNT coatings were found to be 1.6±0.5% and 2.3±0.9% respectively. This indicates that dense coatings can be sprayed which is one of the main advantages of cold spraying. Two types of pores are seen. The first type is between the Al particles and the second type which happens to be the major one is present adjacent to locations where the spray dried agglomerate is entrapped. When the spray dried particles get entrapped between deforming Al splats, the porosity is squeezed out which gets entrapped as the second type of porosity. Kang et al. [16] have used cold spraying to deposit spray dried agglomerates of tungsten and copper. It was found that the porosity was mostly found at the coalesced tungsten particles and that while the spray dried particle had 75 wt.% W, the coating had only 37 wt.% W in it. Fig. 5 shows the SEM of the fracture surface of the Al–0.5CNT coating. Fig. 5a shows an entrapped spray dried particle. Many Al–Si particles are also seen due to disintegration of spray dried particles. Fig. 5b shows Al–Si particles embedded in aluminum matrix with a mechanical bond apparently existing between the two. It is seen that the Al–Si particles penetrate into the Al matrix (marked by the arrow) owing to their high hardness of 1260 MPa, which has an effect of indenting the softer Al matrix. However, most of Al–Si particles are not well bonded to the Al matrix due to the lower amount of energy available after disintegration of the agglomerate.

As a consequence of the disintegration of the spray dried powder, CNTs are fragmented and are evenly distributed in the matrix. It is seen from Fig. 6a that CNTs appear to be homogeneously distributed between the Al splats. Fig. 6b shows CNTs embedded in Al matrix forming a mechanical bond. The bonding between Al and CNTs might not be strong. This is expected since there is no thermal energy input and the occurrence of a chemical reaction between Al and CNT will require some minimum activation energy. Laha et al. [44] have shown theoretically and experimentally that β-SiC forms at the CNT matrix interface during plasma spraying of Al–23 wt.% Si powders with 10 wt.% CNTs which might help in load transfer. The actual values of interfacial strength can be predicted only from bulk tensile test data which will be carried out in the future. Interfacial bond formation is a prerequisite for shear stress transfer and reinforcement of the matrix which is the basis of the shear-lag theory for short fiber reinforced composites. In a recent research, Salas et al. have consolidated Al–CNT mixtures using a shock wave technique [45]. It was observed that most of the CNTs were found at the Al particle triple points. CNTs formed an agglomerated carbonaceous mass and displayed extensive damage. Cold spraying also involves high impact consolidation though less aggressive than shock wave techniques. The deformation and damage of carbon nanotubes in cold sprayed coating is discussed in the next section.

3.4. Deformation and damage of carbon nanotubes

It was observed in most of the fracture surface micrographs that CNT could be retained and uniformly distributed. Most of the visible damage observed was shortening of the length of the nanotubes. Figs. 7 and 8 show the length and diameter of the nanotubes, respectively, as measured from the series of SEM micrographs. The values of the mean and standard deviation of length and diameter of

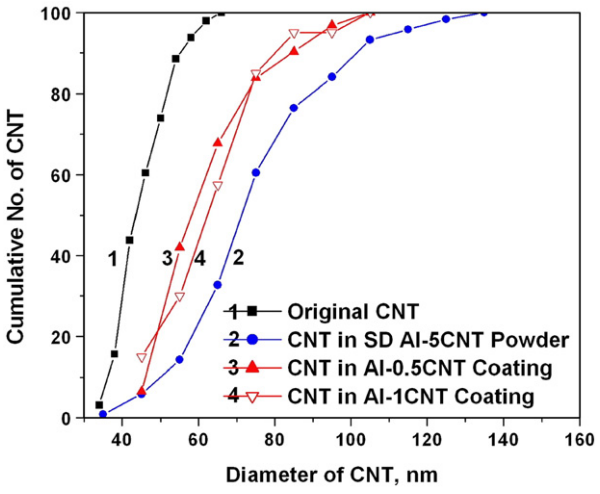

Fig. 8. Diameter of the CNTs at various stages in the fabrication process.

Table 1
Length and diameter of CNTs during various stages of the processing

CNT considered	Length, μm	Diameter, nm
As-received CNT	2.1±0.4	47±7
In spray dried agglomerate	1.3±0.6	78±19
In Al–0.5CNT coating	0.8±0.4	66±15
In Al–1CNT coating	0.85±0.4	68±15

the CNTs during various stages of the processing are tabulated in Table 1. It can be seen that there is a decrease in the length of CNT after spray drying. This shortening happens during mixing operation for the preparation of the slurry used in spray drying. The milling action due to rubbing Al–Si particles might cause breakage of CNT. Chen et al. [46] have also observed shortening of CNTs due to milling in a two roller mill, the extent of which increases by addition of PMMA particles. Also the CNT are observed to be thicker in the spray dried powder. This is because they are covered with the binder used for spray drying. After cold spraying, there is a decrease in the value of both the length and diameter of the CNT. The decrease in diameter means that the binder is ripped off the CNT due to the gas flow, impact and disintegration of the agglomerate and during the rubbing action between particles. There is a noticeable decrease (~30%) in length of the nanotubes.

Fig. 9a and b shows TEM micrographs of fractured end or tips of two different CNTs. As seen in Fig. 9a, after the impact there is a systematic fracture of the concentric tubes which progresses inward until the innermost tube has broken. On the other hand, Fig. 9b shows the fractured tip of a CNT that is uneven or asymmetric with respect to tube axis. Two mechanisms are responsible for the fracture surfaces observed. They are by impact and by shear which are schematically described in Fig. 9c and d respectively. When the spray dried agglomerate strikes the substrate/coating, there is a possibility of a CNT being crushed in between the incoming Al–Si particle and the preceding splat. Depending on whether the Al–Si particle strikes a horizontal or an inclined surface, it will exert impact or shear forces on the nanotube. Both impact and shear is expected to cause fracture in CNT. Impact is expected to result in CNTs with fracture surface that is normal or symmetric to the longitudinal axis while shearing will result in broken CNTs with fracture surfaces that are inclined or asymmetric to the longitudinal axis. A CNT might undergo multiple events of fracture before getting embedded or entrapped within two particles or in porous area between particles created as a result of insufficient deformation.

3.5. Nanoindentation studies on the coatings

Vickers microhardness measured using a LECO M-400 tester with a load of 200 g and 15 s dwell time was found to be 58.7±3.2 VHN and 60.9±2.8 VHN for the Al–0.5CNT and Al–1CNT coating respectively. This corresponds to a small increase in hardness. In order to measure the effect of CNT on the elastic modulus, nanoindentation was carried out. Nanoindentation was carried out on polished cross-section of both coatings. A matrix of 7 (x) 7 indentations (49 indents) was made for Al–0.5CNT coating. Each indent was 10 μm apart. Hence these values are obtained from an area of 70 μm×70 μm. A matrix of 5 (x) 5 indentations (25 indents) representing an area of 50 μm×50 μm was made for Al–1CNT coating. Fewer indents were required for the Al–1CNT coating because there was a lower spread in the values. Fig. 4c and d show that an area of 50 μm×50 μm is representative of multiple splats and features present in the coating that includes, pure Al, Al–Si

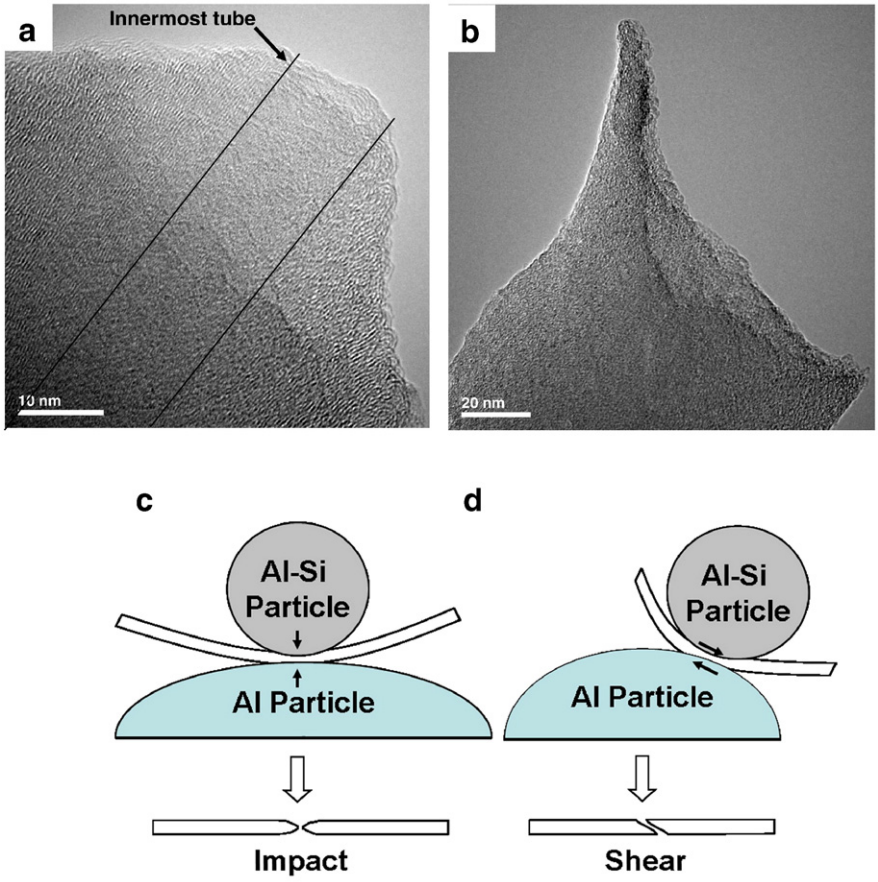

Fig. 9. Transmission electron microscope images showing (a) tip of CNT broken due to impact, and (b) tip of a CNT broken due to shearing. Schematic showing the two mechanisms for fracture of CNTs during cold spraying namely by (c) impact and (d) shear.

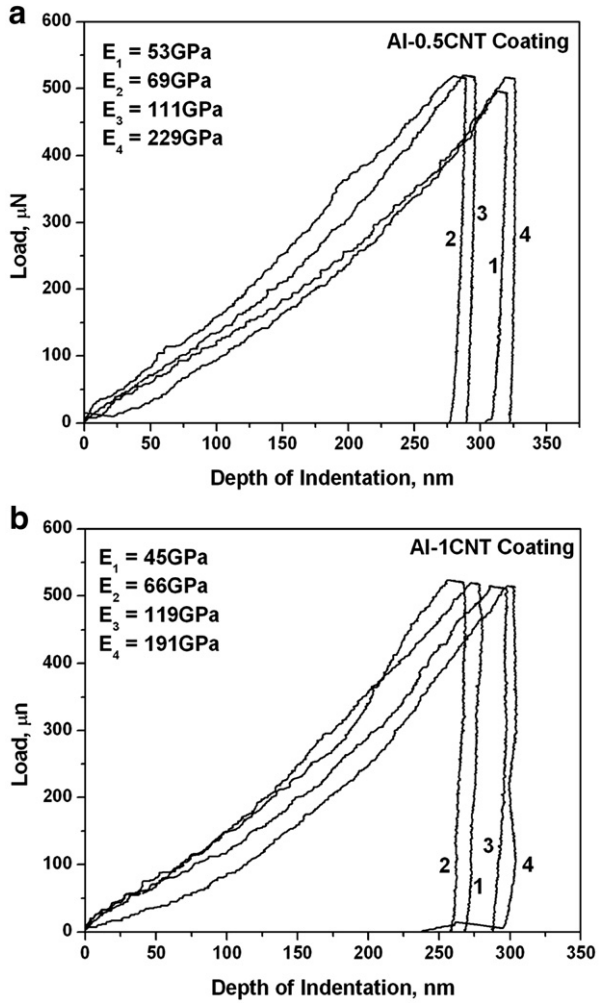

Fig. 10. Load vs. depth curve obtained from the nanoindentation of a) Al–0.5CNT, and b) Al–1CNT coating.

eutectic, porosity and CNTs. In both cases, it was found that there was a distribution in the values of the elastic modulus ranging from 40–220 GPa, though majority of the values ranged between 40 and 120 GPa. Fig. 10 shows the load vs. depth curves for the lowest, highest and close to mean values obtained during the tests for the two samples. The values obtained by nanoindentation are specific to the local microstructure where the indentation was performed. Fig. 11 plots the values of the elastic modulus measured at different locations within the coating in the form of histograms. The mean elastic modulus in both cases is close to 69 GPa which is the elastic modulus of polycrystalline aluminum [47] that makes up for most of the coating microstructure. The elastic modulus of polycrystalline silicon is 115 GPa [47] which is close to the maximum value of elastic modulus measured. Thus an indentation on the Al splat will give a value of 69 GPa but on a Al–Si region will yield a value anywhere between 40 and 115 GPa based on the degree of porosity. It is observed from Fig. 11 that a larger fraction of measured values fall between 40 and 60 GPa (24% for Al–0.5CNT and 44% for Al–1CNT) and 90 and 120 GPa (9% for Al–0.5CNT and 19% for Al–1CNT) range for 1 wt.% CNT-containing coating. This is due to the fact that the volume fraction of porous regions as well as Al–Si particles in the 1 wt.% coating is higher. So statistically it is more probable to encounter such regions while carrying out nanoindentation testing in case of 1 wt.% CNT-containing coating.

Some large values for elastic modulus (155–229 GPa for Al–0.5CNT and 141–191 for Al–1CNT) were also obtained during nanoindentation of the present coatings. These modulus values are significantly higher than the elastic modulus of pure aluminum or silicon. This is due to the presence and the reinforcement action of CNT present in the region. There are four factors which influence the overall elastic modulus at a given location. They are the volume fraction of Al, Al–Si, CNT and porosity present in the coating. The overall volume fraction of silicon in the composite is 0.014 and 0.028 respectively for 10 wt.% and 20 wt.% addition of Al–Si powder to Al. Considering the rule of mixtures to hold true for the reinforcement due to silicon, the value of the elastic modulus of the matrix without CNT is calculated to be 70 GPa. So the reinforcement is mostly due to the presence of CNTs in the matrix. The elastic modulus of the CNT-containing composites calculated using various micromechanical models is presented in Table 2. The elastic modulus value for CNT has been assumed as 950 GPa [23]. It is found that the predicted values from Halpin –Tsai equations and the modified Eshelby [51] method are close to the mean of the measured value. Coleman et al. [22] have observed that the Halpin–Tsai equations for random fiber orientation fit the experimentally measured values well at low volume fraction of reinforcement. Some of the measured values of elastic modulus are low compared to the predicted value. In these calculations the porosity has not been taken into account. The porosity in the present coatings is 1–3 vol.% which is low and is going to have small effect on the overall modulus. However the localized increase in the fractional porosity might have significant effect on values obtained by nanoindentation which is difficult to model. The higher values obtained from nanoindentation reflects the values at different locations which

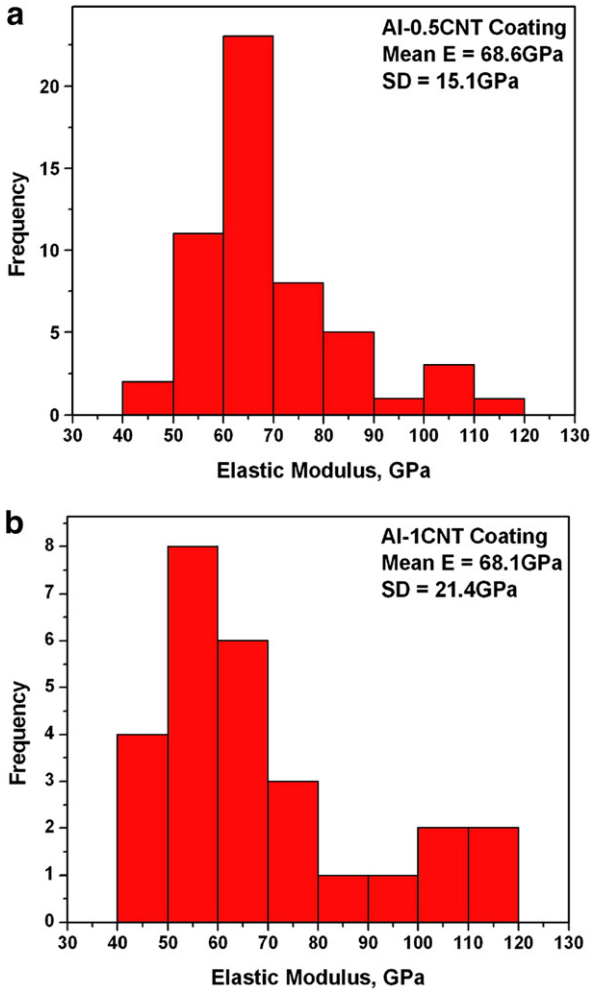

Fig. 11. Histogram of measured values of elastic modulus by nanoindentation for a) Al–0.5CNT, and b) Al–1CNT coating.

Table 2
Elastic modulus of the composite calculated using micromechanical models

Model used	Calculated elastic modulus of composite, GPa	
	Al–0.5CNT	Al–1CNT
Rule of mixture [48]	75	81
Mori–Tanaka [49]	85	86
Hashin–[50]	Lower bound — 85 Upper bound — 88	Lower bound — 86 Upper bound — 91
Halpin–Tsai [22]	72.5	75
Modified Eshelby method [51]	71.5	73.5

might have an increased concentration of CNTs. Ling and Hou [52] have carried out the nanoindentation of Al_2O_3–SiC composites and have found a decrease in the average elastic modulus with an increasing SiC content and a large scatter in data due to porosity. Kim et al. [53] have fabricated fully dense CNT reinforced Cu composites by spark plasma sintering of CNT–Cu powders obtained by molecular level mixing. It was observed that Vickers hardness increases almost linearly by 80% for a 10 vol.% addition of CNTs [53]. Salas et al. [45] have reported a decrease in the Rockwell hardness (Scale E) due to addition of CNT in shock consolidated aluminum. It was found that the CNTs formed carbonaceous aggregates which served as easy sites for failure and delamination [45]. These studies have confirmed that dispersion of CNTs and porosity are very important factors determining the extent of reinforcement achieved. For an over all assessment of the increase in the elastic modulus, bulk tensile testing and/or large area modulus mapping of both coatings will be carried out in our future studies.

4. Conclusions

Aluminum composites reinforced with CNTs were successfully synthesized by cold spraying a blended powder. This comprised pure Al powder and spray dried agglomerates of Al–Si eutectic powder containing either 10 wt.% or 20 wt.% CNTs. Coatings up to 500 μm thick were successfully sprayed onto aluminum alloy AA6061 substrate with overall nominal CNT compositions of 0.5 and 1 wt.%. CNTs are successfully retained and located both between the splat interfaces and also embedded in the matrix. However, CNTs are shortened in length due to fracture that occurs due to impact and shearing between Al–Si eutectic particles and the aluminum matrix. Nanoindentation of the composite yeilded a range of values of the elastic modulus between 40 GPa and 120 GPa. The lower values correspond to the porous regions of the deposit whilst the higher values correspond to the Si rich regions. Some regions had elastic modulus as high as 229 GPa for Al–0.5 wt.% CNT and 191 GPa for Al–1wt.% CNT coating. This is attributed to the reinforcement effect of CNTs and the locally high level of CNTs in the region measured.

Acknowledgments

A. Agarwal and S. R. Bakshi would like to acknowledge funding from the National Science Foundation CAREER Award (NSF-DMI-0547178) and International Research and Education in Engineering (NSF-DMI-0634949). S. R. Bakshi would like to acknowledge the Presidential Enhanced Assistantship from Florida International University. The authors would like to thank Dr. Deen Zhang and Mr. Timothy Price of the University of Nottingham for their help with cold spraying and Prof. T. Hyde for the provision of laboratory facilities at the University of Nottingham.

References

[1] A.P. Alkimov, A.N. Papyrin, V.F. Kosarev, N.I. Nesterovich, and M.M. Shushpanov, U.S. Patent 5302414, April 12 (1994).
[2] H. Assadi, F. Gartner, T. Stoltenhoff, H. Kreye, Acta Mater. 51 (2003) 4379–4394.
[3] M. Grujicic, C.L. Zhao, W.S. DeRosset, D. Helfritch, Mater. Des. 25 (2004) 681–688.
[4] V. Champagne, D. Helfritch, P. Leyman, R. Lempicki, S. Grendahl, Model. Simul. Mater. Sci. Eng. 13 (2005) 1119–1128.
[5] M. Grujicic, C.L. Zhao, W.S. DeRosset, D. Helfritch, Mater. Sci. Eng., A 368 (2004) 222–230.
[6] Chang-Jiu Li, W-Ya Li, Yu-Yue Wang, Guan-Jun Yang, H. Fukanuma, Thin Solid Films 498 (2005) 79–85.
[7] C. Borchers, F. Garner, T. Stoltenhoff, H. Kreye, J. Appl. Phys. 96 (2004) 4288–4292.
[8] T.H. Van Steenkiste, J.R. Smith, R.E. Teets, J.J. Moleski, D.W. Gorkeiwicz, R.P. Tyson, D.R. Marantz, K.A. Kowalsky, W.L. Riggs II, P.H. Zajchowski, B. Pilsner, R.C. McCune, K.J. Barnett, Surf. Coat. Technol. 111 (1999) 62–71.
[9] C-Jiu Li, W-Ya Li, Surf. Coat. Technol. 167 (2003) 278–283.
[10] Chang-Jiu Li, Wen-Ya Li, Yu-Yue Wang, Surf. Coat. Technol. 198 (2005) 469–473.
[11] K. Balani, T. Laha, A. Agarwal, J. Karthikeyan, N. Munroe, Surf. Coat. Technol. 195 (2005) 272–279.
[12] L. Ajdelsztajn, A. Zuniga, B. Jodoin, E.J. Lavernia, Surf. Coat. Technol. 201 (2006) 2109–2116.
[13] J. Wu, J. Yang, H. Fang, S. Yoon, C. Lee, Appl. Surf. Sci. 252 (2006) 7809–7814.
[14] Wen-Ya Li, Chang-Jiu Li, Hanlin Liao, C. Coddet, Appl. Surf. Sci. 253 (2007) 5967–5971.
[15] H. Koivuluoto, J. Lagerbom, P. Vuoristo, J. Therm. Spray Technol. 16 (4) (2007) 488–497.
[16] H-Ki Kang, S.B. Kang, Scr. Mater. 49 (2003) 1169–1174.
[17] H.Y. Lee, S.H. Jung, Soo Yong Lee, Kyung Hyun Ko, Appl. Surf. Sci. 253 (2007) 3496–3502.
[18] Hyung-Jun Kim, Chang-Hee Lee, Soon-Young Hwang, Mater. Sci. Eng., A 391 (2005) 243–248.
[19] P.S. Phani, V. Vishnukanthan, G. Sundararajan, Acta Mater. 55 (2007) 4741–4751.
[20] Kin-Tak Lau, D. Hui, Compos.: Part B 33 (2002) 263–277.
[21] R. Andrews, M.C. Weisenberger, Curr. Opin. Solid State Mater. Sci. 8 (2004) 31–37.
[22] J.N. Coleman, U. Khan, W.J. Blau, Y.K. Gun'ko, Carbon 44 (2006) 1624–1652.
[23] Min-Feng Yu, O. Laurie, M.J. Dyer, K. Moloni, T.F. Kelly, R.S. Ruoff, Science 287 (2000) 637–640.
[24] P. Kim, L. Shi, A. Majumdar, P.L. McEuen, Phys. Rev. Lett. 87 (21) (2001) 215502-1–215502-4.
[25] Guo-Dong Zhan, J.D. Kuntz, J. Wan, A.K. Mukherjee, Nat. Mater. 2 (2003) 38–42.
[26] K. Balani, S.R. Bakshi, Y. Chen, T. Laha, A. Agarwal, J. Nanosci. Nanotechnol. 7 (2007) 1–10.
[27] R. Sivakumar, S. Guo, T. Nishimura, Y. Kagawa, Scr. Mater. 56 (2007) 265–268.
[28] E. Carreño-Morelli, J. Yang, E. Couteau, K. Hernadi, J.W. Seo, C. Bonjour, L. Forro, R. Schaller, Phys. Status Solidi (a) 201 (8) (2004) R53–R55.
[29] Y. Feng, H.L. Yuan, M. Zhang, Mater. Charact. 55 (2005) 211–218.
[30] S. Arai, M. Endo, N. Kaneko, Carbon 42 (2004) 641–644.
[31] X. Chen, J. Xia, J. Peng, W. Li, S. Xie, Comput. Sci. Tech. 60 (2000) 301–306.
[32] K.T. Kim, S.I. Cha, S.H. Hong, S.H. Hong, Mater. Sci. Eng., A 430 (2006) 27–33.
[33] L-Xue Pang, K-Ning Sun, S. Ren, C. Sun, R-Hua Fan, Z-Hua Lu, Mater. Sci. Eng., A 447 (2007) 146–149.
[34] A.M.K. Esawi, M.A. El Borady, Comput. Sci. Tech. 68 (2) (2008) 486–492.
[35] T. Laha, A. Agarwal, T. McKechnie, S. Seal, Mater. Sci. Eng., A 381 (2004) 249–258.
[36] T. Laha and A. Agarwal, Mater. Sci. Eng., A, doi:10.1016/j.msea.2007.07.047.
[37] G. Yu, A. Cao, C.M. Lieber, Nat. Nanotechnol. 2 (2007) 372–377.
[38] D. Zhang, P.H. Shipway, D.G. McCartney, J. Therm. Spray Technol. 14 (2005) 109–116.
[39] R.C. Dykhuizen, M.F. Smith, J. Therm. Spray Technol. 7 (2) (1998) 205–211.
[40] C. Thornton, K.K. Yin, M.J. Adams, J. Phys., D: Appl. Phys. 29 (1996) 424–435.
[41] C. Thornton, L. Liu, Powder Technol. 143–144 (2004) 110–116.
[42] A. Papyrin, V. Kosarev, S. Klinkov, A. Alkhimov, V. Fomin, in: A. Papyrin (Ed.), Cold Spray Technology, Elsevier, 2007, p. 40.
[43] T. Price, PhD thesis University of Nottingham 2008.
[44] T. Laha, S. Kuchibhatla, S. Seal, W. Li, A. Agarwal, Acta Mater. 55 (2007) 1059–1066.
[45] W. Salas, N.G. Alba-Baena, L.E. Murr, Metall. Mater. Trans., A 38 (12) (2007) 2928–2935.
[46] L. Chen, X-Jiang Pang, Q-Tang Zhang, Z-Long Yu, Mater. Lett. 60 (2006) 241–244.
[47] M. Warmuzek, Aluminum–Silicon Casting Alloys: Atlas of Microfractographs, ASM International, 2004, p. 3.
[48] N.E. Dowling, Mechanical Behavior of Materials: Engineering Methods for Deformation, fracture, and fatigue, 129, Prentice Hall, New Jersey, 1993, pp. 191–192, 1st ed.
[49] T. Mori, K. Tanaka, Acta Metall. 21 (1973) 571–574.
[50] Z. Hashin, S. Strikman, J. Mech. Phys. Solids 11 (1963) 127–140.
[51] Y. Chen, K. Balani, A. Agarwal, Appl. Phys. Lett. 91 (2007) 031903.
[52] Z. Ling, J. Hou, Comput. Sci. Tech. 67 (2007) 3121–3129.
[53] K.T. Kim, S.I. Cha, S.H. Hong, Mater. Sci. Eng., A 46 (2007) 449–451.